

Supplementary Information: Deterministic multi-phonon entanglement between two mechanical resonators on separate substrates

Ming-Han Chou,^{1,2,*} Hong Qiao,^{1,†} Haoxiong Yan,¹ Gustav Andersson,¹
Christopher R. Conner,¹ Joel Grebel,^{1,‡} Yash J. Joshi,¹ Jacob M.
Miller,² Rhys G. Povey,² Xuntao Wu,¹ and Andrew N. Cleland^{1,3,§}

¹*Pritzker School of Molecular Engineering,
University of Chicago, Chicago IL 60637, USA*

²*Department of Physics, University of Chicago, Chicago IL 60637, USA*

³*Center for Molecular Engineering and Material Science Division,
Argonne National Laboratory, Lemont IL 60439, USA*

This section provides detailed information about our experimental setup. Device properties and simulation parameters are summarized in Supplementary Tables 1 and 2. In Supplementary Fig. 1, we characterize the lifetime of each mechanical resonator using the associated qubit and coupler. By fitting the qubit excitation probability evolution traces, we extract each resonator’s energy relaxation and dephasing times. Supplementary Fig. 2 outlines the calibration of the displacement pulse amplitude (dpa) and identifies the operational regime where the displacement drive amplitude and average phonon number exhibit a linear relationship, which is the region used for all qubit-resonator entanglement experiments. Supplementary Fig. 3 shows an example of Wigner tomography performed with two non-zero displacement pulses applied to the mechanical resonators, where non-zero probabilities for the higher energy levels are observed, as expected. In Supplementary Fig. 4, we measure a multi-mode mechanical resonator using a similar architecture, demonstrating the potential for scalability of the quantum acoustic system. Finally, Supplementary Fig. 5 provides a detailed electronics and wiring diagram used for the experiments.

* These authors contributed equally to this work; Present address: AWS Center for Quantum Computing, Pasadena, CA 91125, USA

† These authors contributed equally to this work.

‡ Present address: Google, Santa Barbara, California 93117, USA

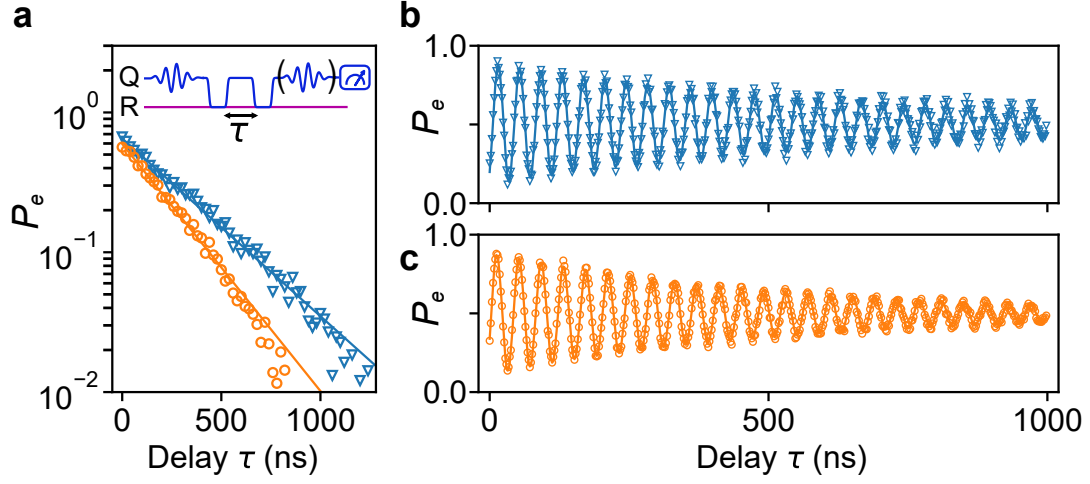
§ anc@uchicago.edu

Qubits	Q_A	Q_B
Qubit idle frequency (GHz)	3.245	3.557
Anharmonicity (MHz)	-207	-196
Intrinsic lifetime T_1 (μs)	40.8	19.3
Ramsey dephasing time $T_{2,R}$ (μs)	2.7	3.0
Readout resonator frequency (GHz)	4.435	4.486
$ g\rangle$ state readout fidelity	0.970	0.976
$ e\rangle$ state readout fidelity	0.953	0.962
$ f\rangle$ state readout fidelity (three state readout)	0.923	0.929
$ f\rangle$ state lifetime (μs)	10.1	10.5
$ e\rangle$ state lifetime during $ e0\rangle \leftrightarrow g1\rangle$ swap (ns)	784	350
$ e\rangle$ state dephasing time during $ e0\rangle \leftrightarrow g1\rangle$ swap (ns)	765	698
SAW resonators	R_A	R_B
Resonator frequency (GHz)	3.027	3.295
Resonator T_1^m (ns)	380	270
Resonator T_2^m (ns)	709	527
Qubit-resonator max coupling g_{ge} (MHz)	5.9	7.1
Experimental g_{ef} (MHz)	3.8	3.8

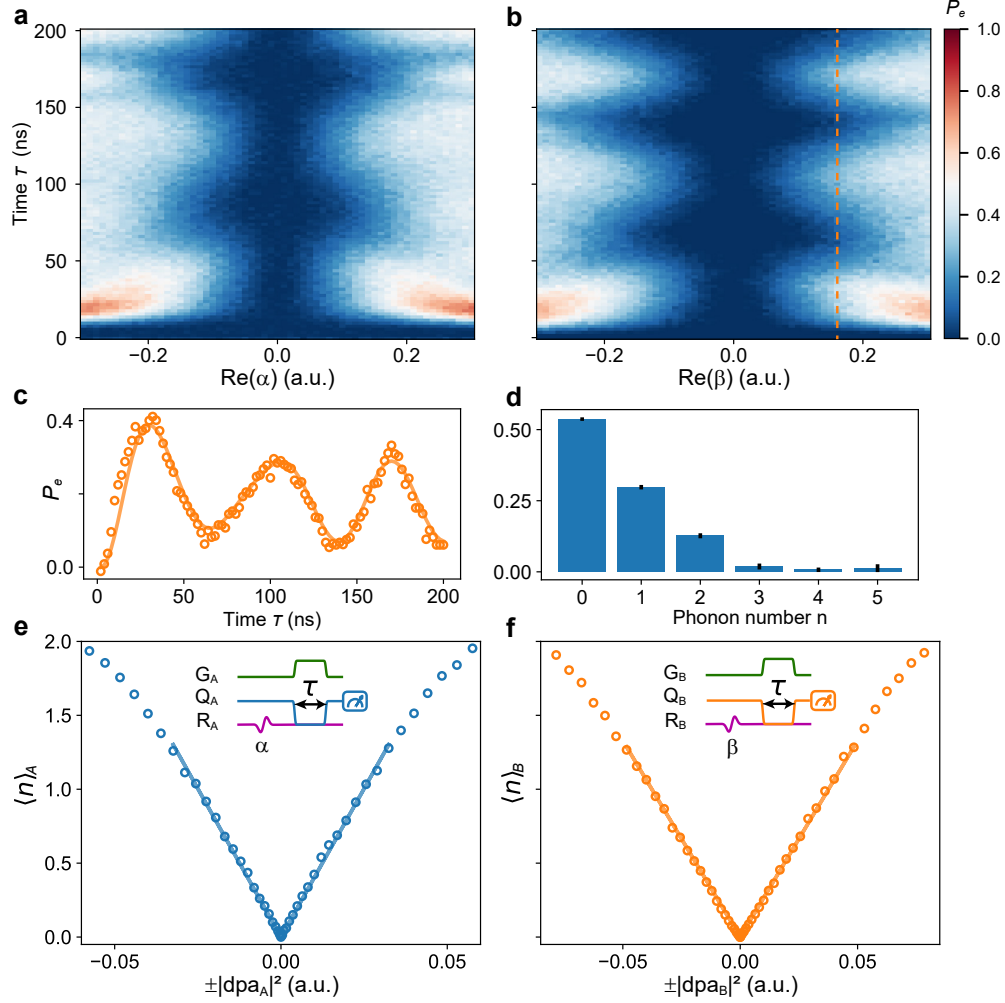
Supplementary Table. 1: **Summary of device parameters.** Qubit lifetimes, dephasing times, and readout fidelities are measured at the qubit idle frequency. $|e\rangle$, $|g\rangle$ state fidelities are the typical fidelities of measuring $|e\rangle$, $|g\rangle$ states when preparing the qubit in the $|e\rangle$, $|g\rangle$ states. $|f\rangle$ state readout fidelities are separately measured in three state readout. When swapping the qubit state $|f\rangle$ into resonator ($|f0\rangle \leftrightarrow |e1\rangle$), the qubit $|e\rangle$ state suffers from non-resonant phonon emission, resulting in a relatively short lifetime (see main text).

SAW resonators	R_A	R_B
SAW wavelength λ_0 (μm)	1.301	1.194
Cavity length (μm)	74.0	69.6
Sound speed (m/s)	3979	
LiNbO ₃ coupling coefficient K^2 (%)	5.4	
Transducer finger pairs	10	
Number of lines in mirror	400	
IDT duty cycle	0.5	
Mirror duty cycle	0.5	
Aperture (μm)	180	
Metal thickness (nm)	10	
IDT reflection coefficient	$-0.042j$	
Mirror reflection coefficient	$-0.0267j$	

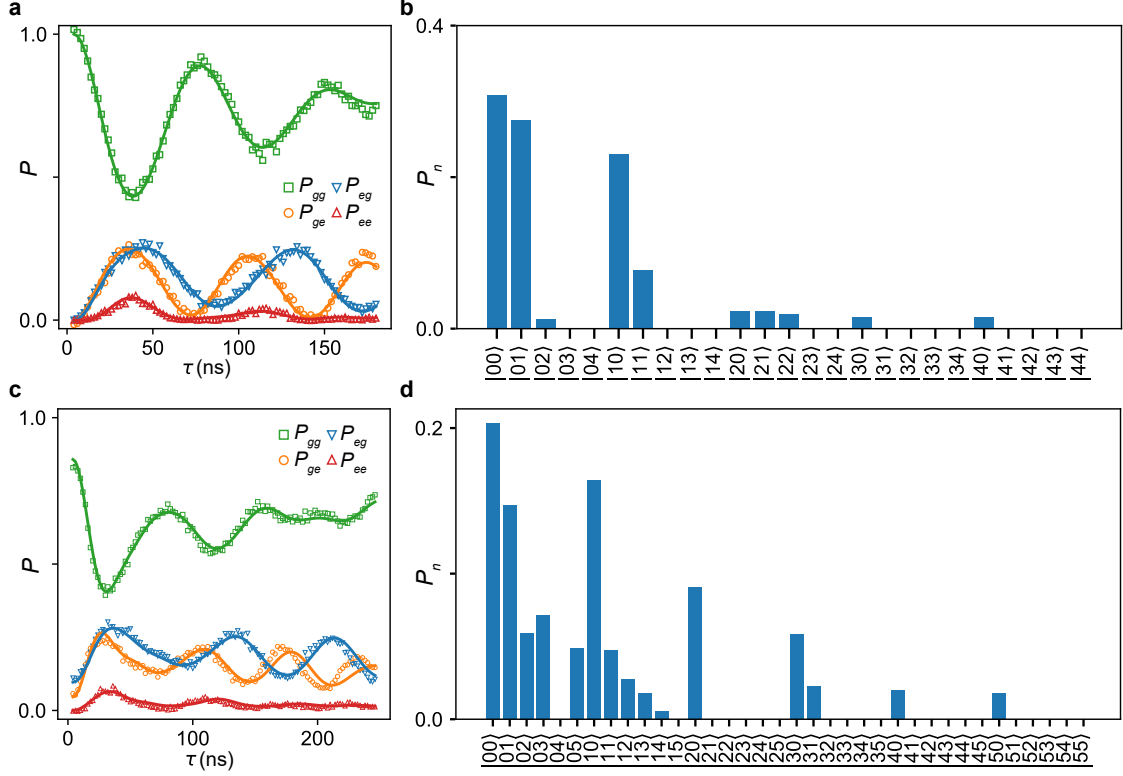
Supplementary Table. 2: **Summary of SAW resonator design and P-matrix model.** We provide the design parameters for each SAW resonator (R_A and R_B) and P-matrix model parameters used for numerical results in Fig. 2a.



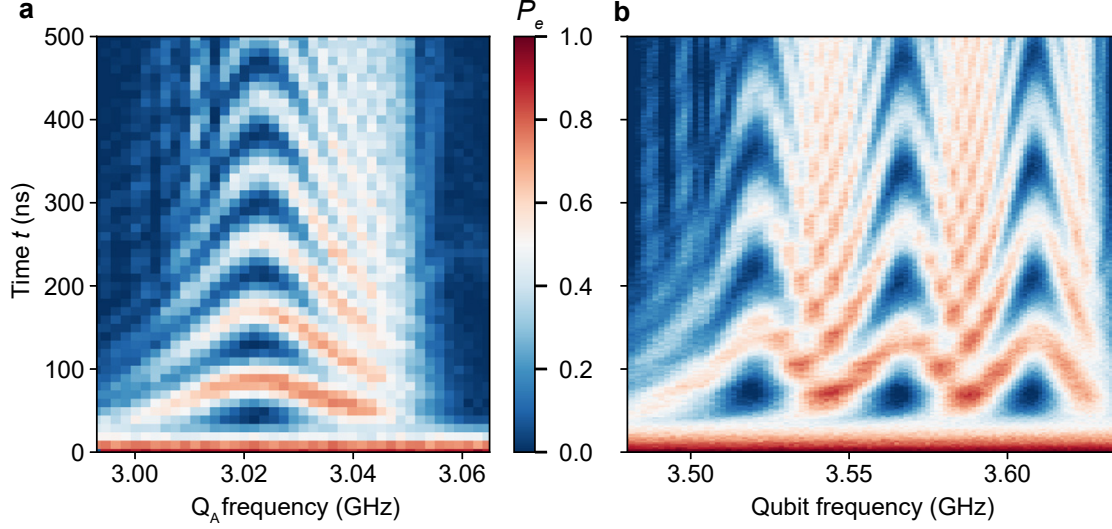
Supplementary Fig. 1: **Mechanical resonator characterization.** Mechanical resonator lifetime (a) and coherence time (b, c) measurements for resonators R_A (blue) and R_B (orange). Inset in panel a shows the pulse sequence for corresponding experiments (coupler control pulses not shown). Solid lines are least-squares fitting results.



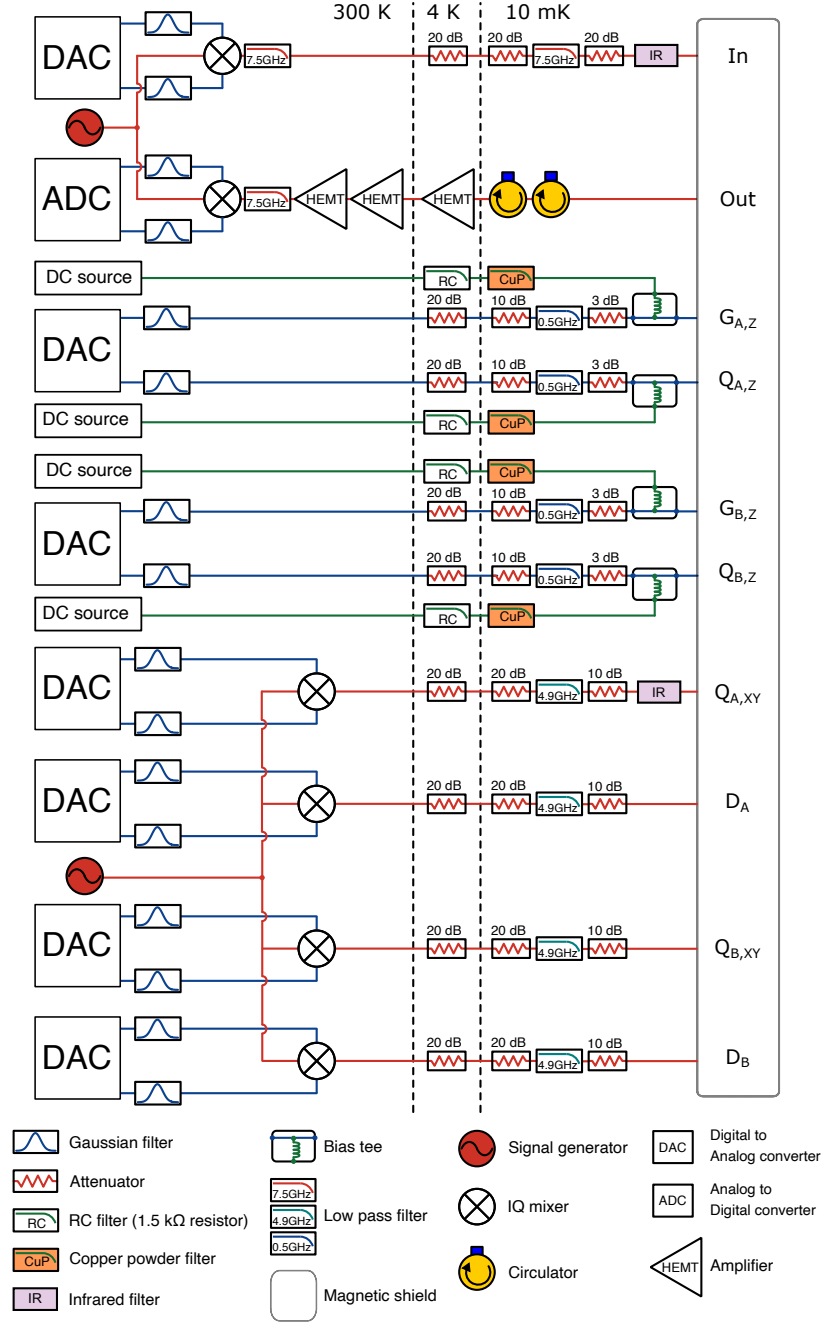
Supplementary Fig. 2: **Displacement pulse calibration.** **a, b,** We displace each mechanical resonator R_A and R_B using a coherent on-resonance drive tone, then measure the average population of the resonator using its associated qubit. The plots show the time-dependent qubit-resonator interactions, for real-only displacement amplitudes α and β (horizontal axis) and interaction times τ (vertical axis). **c, d,** Example fit of the evolution of the phonon number population of resonator R_B , from the vertical orange dashed line cut in **b**. Error bars in panel d are represented by black vertical lines, indicating one standard deviation. **e, f,** In the low phonon number limit, the average phonon number $\langle n \rangle$ scales linearly with the square of the displacement pulse amplitude (dpa). At higher phonon numbers, we attribute the saturation effect to pulse distortion-induced fitting inaccuracies. In the experiment, the displacement pulse amplitudes used are always in the linear range. The average phonon number $\langle n_A \rangle$ and $\langle n_B \rangle$ generated from the respective displacement lines can be estimated from this calibration curve.



Supplementary Fig. 3: **Wigner tomography for non-zero displacement pulses.** **a**, Qubit-resonator swaps for displacements with $\alpha = 0.35$ and $\beta = -0.0271 - 0.258i$ for resonators R_A and R_B respectively. Data are joint qubit measurements. **b**, Fitted probabilities for the corresponding joint mechanical resonator populations. For the fits, we use each resonator's lowest five energy levels. **c**, Qubit-resonator swaps for non-zero displacements with $\alpha = 0.5$ and $\beta = 0.5$, here for analysis of the $N = 2$ N00N state. **d**, Fit joint mechanical resonator population probabilities, for the data in **c** using six resonator levels in each resonator. For Fig. 3 in the main text, we only show three energy levels in each resonator for the Bell state resonator populations, and in Fig. 4, four energy levels in each resonator for the N00N state resonator populations. Here we show all the resonator levels used in the fitting for tomography of the Bell states (5 levels) and N00N states (6 levels).



Supplementary Fig. 4: **Qubit-resonator Rabi swaps with a single mode and a multimode mechanical resonator.** **a**, Rabi swap measurement with resonator R_A , which has a single resonant mode. **b**, Qubit-resonator Rabi swaps with a different mechanical resonator with three distinct SAW resonances, using a device design similar to that given in the main text. The distance between the two acoustic mirrors is about $130\mu\text{m}$, increasing the cavity length and decreasing the FSR to 44 MHz. This illustrates the scalability of this architecture to multi-mode, multi-chip formats.



Supplementary Fig. 5: Wiring diagram for the experiments described in the main text. The input (“In”) and output (“Out”) lines are used for qubit state readout. The qubit control lines include an XY line for exciting each qubit ($Q_{A,XY}$ and $Q_{B,XY}$), and a Z line for changing each qubit’s frequency ($Q_{A,Z}$ and $Q_{B,Z}$). The couplers’ control lines ($G_{A,Z}$ and $G_{B,Z}$) are used for adjusting the phase of each variable coupler’s Josephson junction and thus the coupling strength between each qubit and its associated mechanical resonator. The displacement lines (D_A and D_B) are used for applying coherent pulses to each resonator for Wigner tomography.